SCIENTIFIC REPORTS

OPEN

SUBJECT AREAS:
MATERIALS SCIENCE
INORGANIC CHEMISTRY
ENVIRONMENTAL CHEMISTRY
BATTERIES

Received
9 August 2012

Accepted
14 September 2012

Published
4 October 2012

Correspondence and requests for materials should be addressed to K.K. (matlgen1@snu.ac.kr)

Tailoring a fluorophosphate as a novel 4 V cathode for lithium-ion batteries

Young-Uk Park[1], Dong-Hwa Seo[1], Byoungkook Kim[2], Kun-Pyo Hong[3,4], Hyungsub Kim[1], Seongsu Lee[3], Rana A. Shakoor[5], Keiichi Miyasaka[5], Jean-Marie Tarascon[6] & Kisuk Kang[1,7]

[1]Department of Materials Science and Engineering, Seoul National University, Gwanak-ro 1, Gwanak-gu, Seoul 151-742, Korea, [2]Research Analysis Center, KAIST, Daehak-ro 291, Yuseong-gu, Daejeon 305-701, Korea, [3]Korea Atomic Energy Research Institute, P.O. Box 105, Yuseong-gu, Daejeon 305-600, Korea, [4]Graduate School of Green Energy Technology, Chungnam National University, Daehak-ro 99, Yuseong-gu, Daejeon 305-764, Korea, [5]Graduate School of EEWS (WCU), KAIST, Daehak-ro 291, Yuseong-gu, Daejeon 305-701, Korea, [6]Université de Picardie Jules Verne, CNRS UMR 7314, 33 rue Saint Leu, 80039 Amiens, France, [7]Research Institute of Advanced Materials (RIAM), Department of Materials Science and Engineering, Seoul National University, Gwanak-ro 599, Gwanak-gu, Seoul 151-742, Korea.

Lithium-ion batteries, which have been widely used to power portable electronic devices, are on the verge of being applied to new automobile applications. To expand this emerging market, however, an electrode that combines fast charging capability, long-term cycle stability, and high energy density is needed. Herein, we report a novel layered lithium vanadium fluorophosphate, $Li_{1.1}Na_{0.4}VPO_{4.8}F_{0.7}$, as a promising positive electrode contender. This new material has two-dimensional lithium pathways and is capable of reversibly releasing and reinserting ~1.1 Li^+ ions at an ideal 4 V (versus Li^+/Li) to give a capacity of ~156 mAh g^{-1} (energy density of 624 Wh kg^{-1}). Moreover, outstanding capacity retentions of 98% and 96% after 100 cycles were achieved at 60°C and room temperature, respectively. Unexpectedly high rate capability was delivered for both charge and discharge despite the large particle size (a few microns), which promises further enhancement of power density with proper nano-engineering.

Rapidly-growing demand for better-performing lithium-ion batteries has driven researchers and engineers to intensively search for new materials having enhanced electrochemical properties[1,2]. As the key technology for further development of hybrid or all-electric vehicles, lithium-ion batteries having higher power and energy density, safety, and cycle stability need to be developed. With this goal in mind, several groups of new polyanionic compounds have been discovered, including fluorosulfates[3–5], pyrophosphates[6], silicates[7–9], borates[10–12] and fluorophosphates[13–17]. The diverse electrochemical properties of these compounds are critically affected by the species of polyanion and how they, as the building blocks, are arranged in the crystal lattice. The presence of polymorphism with one-, two-, or three-dimensional diffusional frameworks along with tunable redox potentials from the varying inductive effects of the polyanions offers great flexibility in designing new electrode materials[3–21].

Extensive research has been reported recently on polyanion-based cathodes[3–24]. Earlier studies on sodium super ionic conductors (NASICONs) have shown that their open framework is exceedingly advantageous for fast diffusion of mobile ions; they can be used as the electrode for rechargeable batteries and even as the solid-state electrolyte[18,19,25–28]. However, despite their fast ionic conduction, the heavy framework of typical NASICON-type compounds significantly lowers the energy density and makes them less attractive as an electrode. Rapid ionic conduction could be combined with multivalent transition metals that can contribute more than one-electron transfer during lithiation and delithiation, which would result in a strong contender to commercially available electrodes. While attempts have been made to use two-electron redox couples such as V^{3+}/V^{5+} in (fluoro)phosphates, the additional capacity from V^{4+}/V^{5+} has been only partially accessible, even at slow rates, and other drawbacks such as high polarization and poor reversibility have been reported as well[16,20–22].

To combine the high ionic conduction of an open framework with a multivalent redox center, we focused on a vanadium-containing fluorophosphate compound in this study. Although sodium vanadium fluorophosphate, $Na_{1.5}VPO_5F_{0.5}$, has shown unsatisfactory electrochemical performance[29], we chose it as a starting material because of its many attractive features: (i) it contains 1.5 mobile ions (Na^+) per transition metal, (ii) it possesses a multivalent transition metal ion, (iii) it has an open crystal structure, and (iv) it has a relatively high voltage of ca. 3.8 V (vs. Na^+/Na). However, the multivalency of the vanadium ion (from +3 to +5)[30] is counterbalanced by the initial valence of +4 in the material. Cathode operation of this material in rechargeable batteries contributes only one electron via the V^{4+}/V^{5+} redox reaction, and results in limited capacity (ca. 130 mAh g^{-1}), even though more

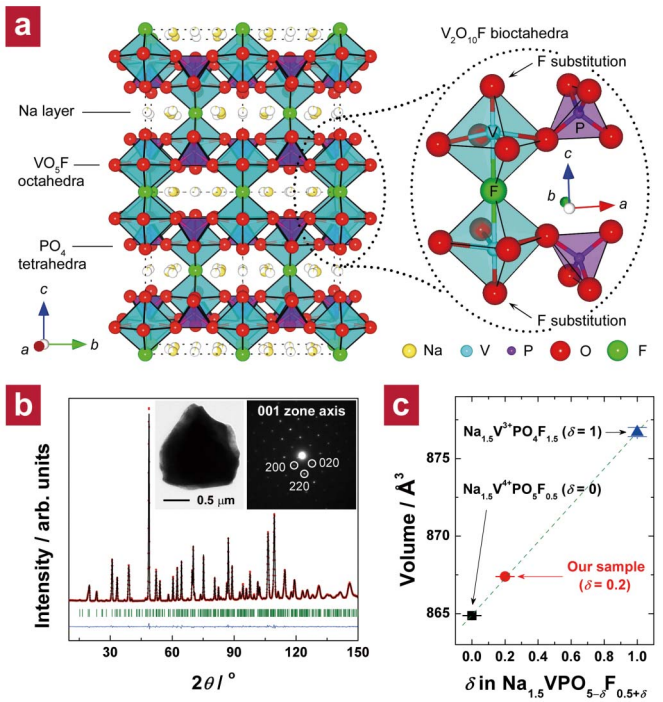

Figure 1 | Structural characterization of the fluorinated $Na_{1.5}VPO_{4.8}F_{0.7}$. (a) Illustration of the crystal structure of the pristine Na phase ($Na_{1.5}VPO_5F_{0.5}$). An enlarged scheme at the right side depicts $V_2O_{10}F$ bioctahedra with corner-sharing PO_4 tetrahedral units. Na, V, P, O, and F atoms are shown in yellow, cyan, purple, red, and green, respectively. (b) ND pattern of the fluorinated Na phase ($Na_{1.5}VPO_{4.8}F_{0.7}$) and its Rietveld refinement with observed data points (red dots), calculated pattern (black line), difference curve (blue line), and Bragg positions (green bars); lattice parameters in the space group $P4_2/mnm$ are $a = b = 9.0332(1)$ Å, $c = 10.6297(2)$ Å, and $V = 867.37(2)$ Å^3. The inset shows a bright-field TEM image of a $Na_{1.5}VPO_{4.8}F_{0.7}$ particle (left) and its corresponding selected-area electron diffraction (SAED) pattern (right); most microcrystallites were single-crystalline (i.e., only spot patterns were detected). (c) Unit cell volumes of $Na_{1.5}VPO_5F_{0.5}$ (■), $Na_{1.5}VPO_4F_{1.5}$ (▲), and $Na_{1.5}VPO_{4.8}F_{0.7}$ (●) by ND analysis. Lattice parameters of $Na_{1.5}VPO_5F_{0.5}$ ($P4_2/mnm$) are $a = b = 9.0257(1)$ Å, $c = 10.6166(2)$ Å, and $V = 864.87(2)$ Å^3; lattice parameters of $Na_{1.5}VPO_4F_{1.5}$ ($P4_2/mnm$) are $a = b = 9.034(3)$ Å, $c = 10.740(8)$ Å, and $V = 876.7(3)$ Å^3.

than one Na^+ ion per transition metal exists in the structure. Further utilization of the vanadium redox reaction below +4 by inserting additional Na^+ ions into the structure has led to a substantially lower voltage that is practically unacceptable. Instead, we adjusted the stoichiometric ratio of oxygen and fluorine in the material and kept the original structure intact. The difference in the oxidation states of F^- vs. O^{2-} could lower the initial valence of the vanadium ion. Moreover, a higher inductive effect with more fluorine-containing polyanion groups in the structure could compensate for the low V^{3+}/V^{4+} redox potential and offer a higher average voltage. We report here that the lithium derivative of this sodium phase obtained from ion-exchange (*Chimie Douce*) between Na^+ and Li^+ has excellent performance as a cathode material, reversibly releasing and reinserting ca. 1.1 Li^+ ions with the V^{3+}/V^{5+} redox reaction at an ideal 4 V in the lithium cell.

Results

Fluorination of the pristine Na phase. $Na_{1.5}VPO_5F_{0.5}$ has a pseudo-layered structure in which the sodium and vanadium layers are roughly separated in an alternate manner along *c* direction (Figure 1a). The framework is made up of VO_5F octahedra and PO_4 tetrahedra units, where two VO_5F octahedra are linked by a bridging fluorine ion to form a $V_2O_{10}F$ bioctahedron[29]. The $V_2O_{10}F$ bioctahedral units are repeatedly connected in *ab* plane via PO_4 tetrahedra sharing oxygen atoms to thereby construct an open framework having a layer-like spacing into which Na^+ ions are intercalated. Our synthesis strategy was to create an appropriate stoichiometric ratio of fluorine and oxygen in $Na_{1.5}VPO_5F_{0.5}$ so that the redox range of vanadium ions was widened below +4 at a reasonably high potential. Starting from $Na_{1.5}VPO_5F_{0.5}$, we tried to increase the degree of fluorination (δ) in $Na_{1.5}VPO_{5-\delta}F_{0.5+\delta}$ by increasing the portion of V^{3+} precursor with a sufficient amount of fluorine-containing precursor, as described in the Methods section. We found that V^{3+} ions prefer F^- ions as the anions constituting the $V_2O_{10-x}F_{1+x}$ bioctahedron than V^{4+} ions due to the charge balance. Hence, by changing the ratio of V^{3+} to V^{4+} precursors, we could control δ. Here, we describe the results of the sample that was shown to have an optimum degree of fluorination, $\delta = 0.2$ (see Chapter 1 in the Supplementary Information for details on stoichiometry optimization).

The phase-pure $Na_{1.5}VPO_{5-\delta}F_{0.5+\delta}$ was successfully obtained, and all reflections in its neutron diffraction (ND) pattern were completely indexed with a space group of $P4_2/mnm$, as shown in Figure 1b (see Chapter 2 in the Supplementary Information for details on the structural refinement). Elemental analysis of the micron-sized Na phase (inset of Figure 1b) by inductively coupled plasma (ICP) and energy-dispersive X-ray spectroscopy (EDS) revealed the detailed composition, i.e., $Na_{1.48(\pm0.02)}V_{1.00}P_{1.00(\pm0.01)}O_{4.78(\pm0.06)}F_{0.74(\pm0.04)}$, hereafter called $Na_{1.5}VPO_{4.8}F_{0.7}$ for convenience (see Chapter 1 in the Supplementary Information for details). Both the decreased O/V ratio and the increased F/V ratio suggested partial replacement of fluorine ions (F^-) for oxygen ions (O^{2-}), which led to a less negatively charged anion group in the structure. X-ray photoelectron spectroscopy (XPS) results (see Supplementary Figure S4) suggested that the fluorine ions replaced those oxygen ions that lie in the two terminal positions of the $V_2O_{10}F$ bioctahedra (denoted by arrows in Figure 1a). By plotting unit cell volumes of two samples having extreme degrees of fluorination ($\delta = 0$ and 1) and our sample ($\delta = 0.2$), we found a linear relationship between δ and cell volume (Figure 1c). This suggests that our sample is a solid-solution phase between $Na_{1.5}V^{4+}PO_5F_{0.5}$ and $Na_{1.5}V^{3+}PO_4F_{1.5}$ with a ratio of 4:1.

Evidence for reduced oxidation state of vanadium in $Na_{1.5}VPO_{4.8}F_{0.7}$. By altering the polyanion group from $[PO_5F_{0.5}]^{5.5-}$ to $[PO_{4.8}F_{0.7}]^{5.3-}$, we could effectively reduce the overall oxidation state of vanadium while maintaining structural integrity. ^{23}Na magic angle spinning (MAS) nuclear magnetic resonance (NMR) spectra of the three samples (Figure 2a) support our claim. The ^{23}Na MAS NMR spectrum of our sample (middle spectrum) shows two major Fermi contact shifts at 70 and 112 ppm, whereas the others exhibit a single Fermi contact shift (e.g., 71 ppm for $Na_{1.5}V^{4+}PO_5F_{0.5}$ and 136 ppm for $Na_{1.5}V^{3+}PO_4F_{1.5}$; this difference can be explained by the fact that V^{3+} ions generally cause a more positive Fermi contact shift than V^{4+} ions by tens of ppm[31,32]). We believe that two paramagnetic sources (V^{4+} and V^{3+} ions) having different number of unpaired electrons are attributable to two dissimilar Fermi contact shifts (70 and 112 ppm), respectively, in the middle spectrum. The average oxidation state of vanadium in $Na_{1.5}V^{3.8+}PO_{4.8}F_{0.7}$ determined by the double titration method was ca. +3.8, which corresponds to that in a 4:1 mixture of V^{4+} and V^{3+} ions (see Chapter 3 in the Supplementary Information for details). This result is in good agreement with the observation that the intensity of the peak at 70 ppm was 3–4 times higher than that at 112 ppm in the ^{23}Na MAS NMR spectrum of $Na_{1.5}V^{3.8+}PO_{4.8}F_{0.7}$. More detailed NMR studies are in progress.

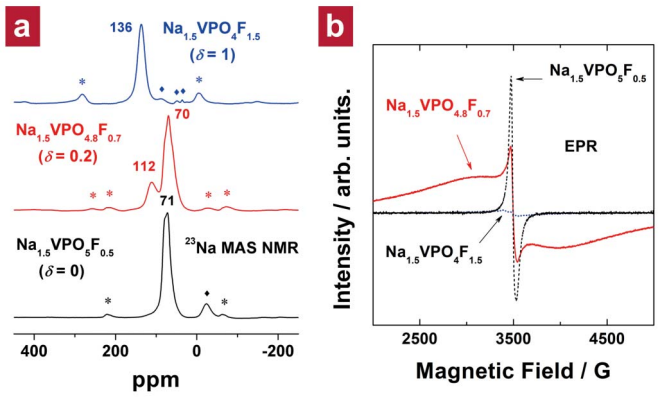

Figure 2 | NMR and EPR spectra of the fluorinated $Na_{1.5}VPO_{4.8}F_{0.7}$. (a) ^{23}Na MAS NMR spectra of $Na_{1.5}V^{4+}PO_5F_{0.5}$ (bottom), $Na_{1.5}V^{3.8+}PO_{4.8}F_{0.7}$ (middle), and $Na_{1.5}V^{3+}PO_4F_{1.5}$ (top). Spinning sidebands are marked with asterisks. Small isotropic peaks (denoted as ◆) could not be assigned. (b) EPR spectra of $Na_{1.5}V^{4+}PO_5F_{0.5}$ (black dashed line), $Na_{1.5}V^{3.8+}PO_{4.8}F_{0.7}$ (red solid line), and $Na_{1.5}V^{3+}PO_4F_{1.5}$ (blue dotted line).

To further probe the substitution, we carried out electron paramagnetic resonance (EPR) experiments (Figure 2b) on those three samples. The EPR spectrum of $Na_{1.5}V^{4+}PO_5F_{0.5}$ was very intense, and the shape was in good agreement with a previous report[33]. However, the EPR signal of $Na_{1.5}V^{3+}PO_4F_{1.5}$ was negligible, which can be explained by the fact that V^{3+}, a non-Kramer's ion with integral J in LS coupling[34], is silent under conventional EPR experimental conditions[35]. On the contrary, the EPR spectrum of our sample, $Na_{1.5}V^{3.8+}PO_{4.8}F_{0.7}$, showed a broad peak, unlike that of $Na_{1.5}V^{4+}PO_5F_{0.5}$ or $Na_{1.5}V^{3+}PO_4F_{1.5}$. It resembles the EPR spectra of $Li_xV_2(PO_4)_3$ phases (x = 2.0 and 2.5) in which V^{3+} and V^{4+} ions coexist[36], implying the coexistence of V^{3+}/V^{4+} ions in our sample.

Na^+/Li^+ ion-exchange for lithium derivative of $Na_{1.5}VPO_{4.8}F_{0.7}$. Ion exchange is an effective way to synthesize a new metastable phase without causing much structural change to the pristine structure[26,37,38]. Using a Na^+/Li^+ ion-exchange method, we successfully prepared an isostructural lithium derivative of $Na_{1.5}VPO_{4.8}F_{0.7}$ (see Supplementary Table S4 for details). According to ICP elemental analysis, ca. 1.1 Na^+ ions were replaced by Li^+ ions without affecting the other elements; the overall composition was $Li_{1.1}Na_{0.4}VPO_{4.8}F_{0.7}$.

Detailed structural analysis of the new lithium phase was carried out using ND and solid-state ^{6}Li and ^{23}Na NMR spectroscopies. All reflections of $Li_{1.1}Na_{0.4}VPO_{4.8}F_{0.7}$ observed in the ND pattern (Figure 3a) could be indexed in the space group $P4_2/mnm$. All Miller indices (hkl) of the structure matched those of $Na_{1.5}VPO_{4.8}F_{0.7}$, indicating that the isostructural lithium derivative was obtained (see Chapter 5 in the Supplementary Information for details on the refinement). $Na_{1.5}VPO_{4.8}F_{0.7}$ and $Li_{1.1}Na_{0.4}VPO_{4.8}F_{0.7}$ particles had similar morphology, with sizes in the range of ca. 1–5 μm (inset of Figure 3a). Figure 3b shows that the observed micron-sized crystallites were single crystals rather than agglomerates of nanocrystals [see Figure S7 in the Supplementary Information for more transmission electron microscopy (TEM) images].

The local lithium environments in $Li_{1.1}Na_{0.4}VPO_{4.8}F_{0.7}$ were investigated by ^{6}Li MAS NMR (see Chapter 7 in the Supplementary Information for more information on ^{23}Na MAS NMR). The ^{6}Li MAS NMR spectrum (Figure 3c) suggests the existence of two types of local environments for lithium in the structure, reminiscent of the two kinds of sodium sites in the parent sodium phase. The signal at 25.5 ppm is significantly more intense than the signal at 0 ppm, indicating that one of two crystallographic sites for alkali ions is preferentially occupied by Li^+ ions. This preferential occupation of Li^+ ions in one alkali-metal site is consistent with the ND refinement result (see

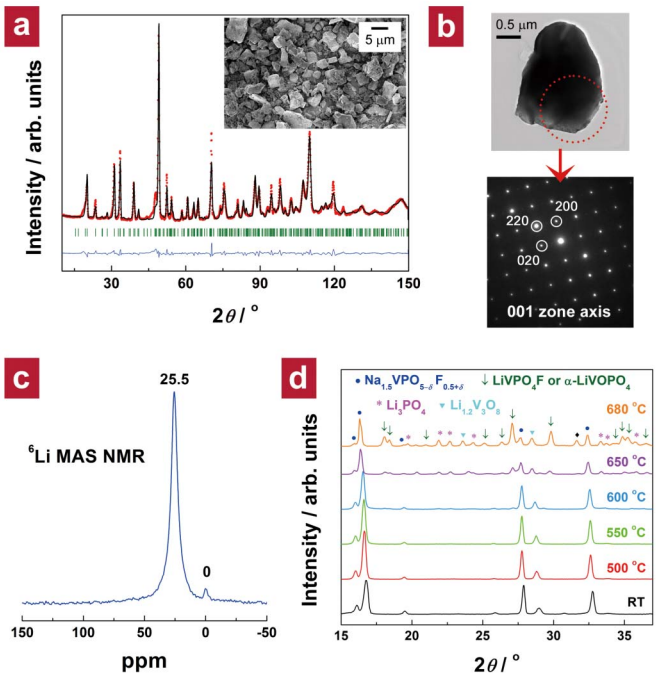

Figure 3 | Material characterization of $Li_{1.1}Na_{0.4}VPO_{4.8}F_{0.7}$. (a) ND pattern of $Li_{1.1}Na_{0.4}VPO_{4.8}F_{0.7}$ and its Rietveld refinement in the $P4_2/mnm$ space group with observed data points (red dots), calculated pattern (black line), difference curve (blue line), and Bragg positions (green bars); lattice parameters are $a = b$ = 8.9836(6) Å, c = 10.4483(8) Å, and V = 843.24(9) Å^3. The unit cell volume was significantly reduced from 867.37(2) Å^3 for $Na_{1.5}VPO_{4.8}F_{0.7}$ to 843.24(9) Å^3 for the new lithium phase because of the smaller ionic radius of Li^+ ion. The inset shows a scanning electron microscopy (SEM) image (magnification: ×5,000). (b) A bright-field TEM image of a micron-sized particle (top) and its corresponding SAED pattern (bottom). (c) ^{6}Li MAS NMR spectrum of $Li_{1.1}Na_{0.4}VPO_{4.8}F_{0.7}$. (d) Temperature-controlled XRD patterns of $Li_{1.1}Na_{0.4}VPO_{4.8}F_{0.7}$. A reflection denoted as ◆ could not be identified.

Supplementary Table S6) and demonstrates that most Li^+ ions reside in the original Na1 site, while the Na2 sites remained mainly occupied by Na^+ ions.

The thermal phase stability of $Li_{1.1}Na_{0.4}VPO_{4.8}F_{0.7}$ was evaluated by temperature-controlled X-ray diffraction (XRD) (Figure 3d). Increasing temperature above 600°C triggered phase separation into a sodium phase ($Na_{1.5}VPO_{5-\delta}F_{0.5+\delta}$) and lithium phase (tavorite $LiVPO_4F$ or triclinic α-$LiVOPO_4$). This suggests that sodium and lithium phases crystallize in different structures having dissimilar stoichiometries in the "Na(Li)–V–P–O–F" system under conventional high-temperature synthesis conditions. Metastable phases obtained from low-temperature *Chimie Douce* routes are often susceptible to thermal degradation upon slight heat treatment. However, we found that the $Li_{1.1}Na_{0.4}VPO_{4.8}F_{0.7}$ phase was thermally stable up to 550°C, which indicates that various low-temperature synthetic techniques, such as ionothermal processes[3–5,39], can be applied to the synthesis of $Li_{1.1}Na_{0.4}VPO_{4.8}F_{0.7}$.

Electrochemical performance of $Li_{1.1}Na_{0.4}VPO_{4.8}F_{0.7}$. The electrochemical properties of $Li_{1.1}Na_{0.4}VPO_{4.8}F_{0.7}$ were examined in a Li cell. The quasi-equilibrium profile obtained by the galvanostatic intermittent titration technique (GITT) at 60°C shown in Figure 4a exhibited an average voltage of ca. 3.95 V. The low-current charge and discharge via the GITT mode exhibited a low polarization and yielded a capacity approaching the theoretical capacity for $Li_{1.1}Na_{0.4}VPO_{4.8}F_{0.7}$, 156 mAh g^{-1} (equivalent to insertion/deinsertion of 1.1 Li^+ ions per formula unit). This clearly indicates more than one lithium ion contributes to the capacity through the widened $V^{3.8+}/V^{5+}$ redox

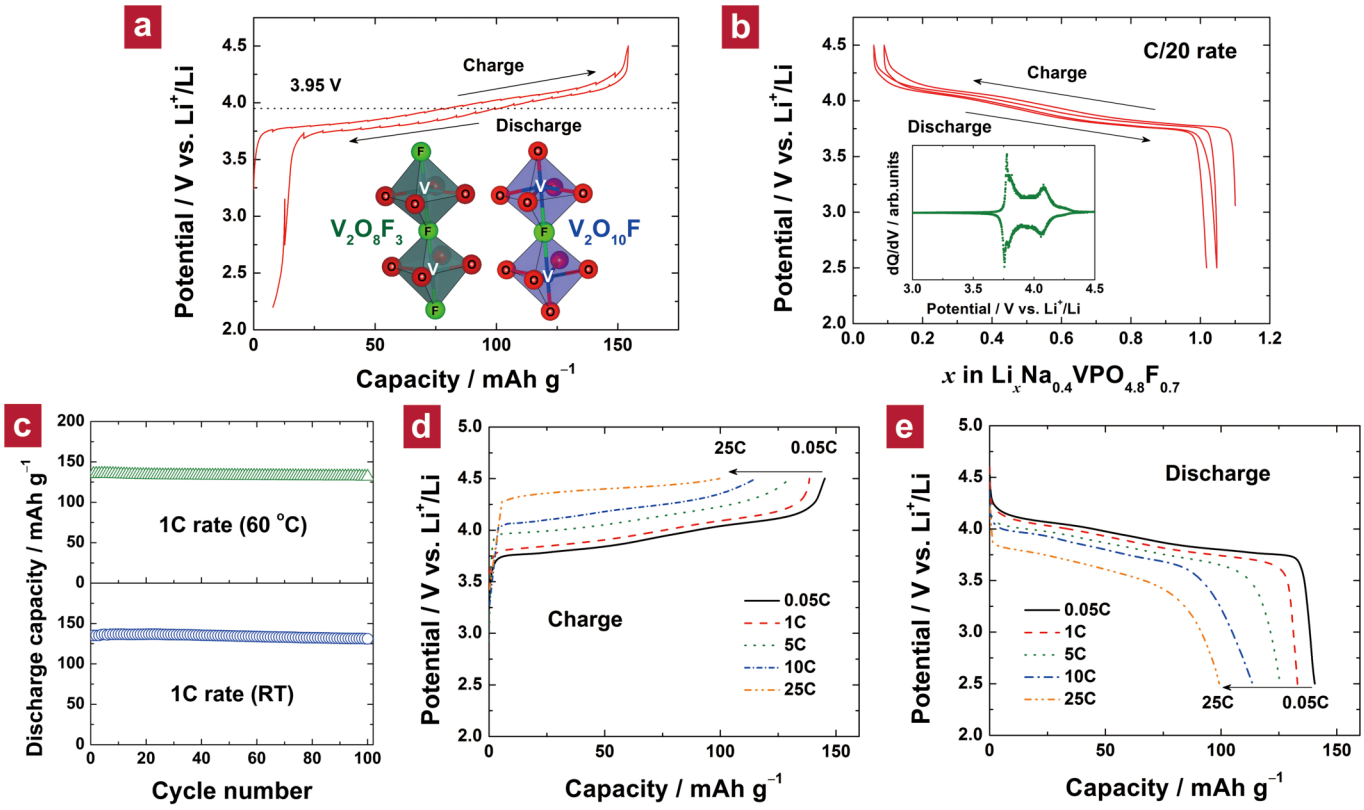

Figure 4 | Electrochemical characterization of $Li_{1.1}Na_{0.4}VPO_{4.8}F_{0.7}$. (a) GITT curve in charge and discharge modes at 60°C. Note that no clear separation was observed between redox potentials of V^{3+}/V^{4+} and V^{4+}/V^{5+} in this material. In fact, the redox potential of V^{3+}/V^{4+} in $V_2O_8F_3$ of $Na_{1.5}V^{3+}PO_4F_{1.5}$ (left inset) is ca. 3.9 V vs. Na^+/Na (ref. 50) and that of V^{4+}/V^{5+} in $V_2O_{10}F$ of $Na_{1.5}V^{4+}PO_5F_{0.5}$ (right inset) is ca. 3.8 V vs. Na^+/Na (ref. 29). We believe that the larger inductive effect in the $V_2O_8F_3$ bioctahedron having more fluorine atoms increased the redox potential of V^{3+}/V^{4+} up to that of V^{4+}/V^{5+}. (b) Galvanostatic charge/discharge curves for the first two cycles at the C/20 rate. 1C corresponds to 156 mA g^{-1}. The inset shows the corresponding dQ/dV curve. Two major peaks were reversibly detected at ca. 3.8 and 4.1 V, whose origin is under investigation. (c) Cyclability over 100 cycles of galvanostatic charge/discharge at the 1C rate at room temperature (bottom) and at an elevated temperature of 60°C (top). (d) The charge and (e) discharge curves for various C rates.

reaction achieved by tailoring the pristine $Na_{1.5}VPO_5F_{0.5}$. The $Na_{1.5}V^{4+}PO_5F_{0.5}$ and its lithium derivative ($LiNa_{0.5}V^{4+}PO_5F_{0.5}$) with a V^{4+}/V^{5+} redox couple can theoretically deliver only ca. 130 mAh g^{-1} and 141 mAh g^{-1}, respectively. Tailoring the pristine fluorophosphate material as the 4 V electrode with the capacity of 156 mAh g^{-1} makes this material a strong alternative to other known cathode materials: $LiCoO_2$ (4 V, ca. 160 mAh g^{-1})[40], $LiFePO_4$ (3.45 V, ca. 170 mAh g^{-1})[41], $LiMn_2O_4$ (4 V, ca. 120 mAh g^{-1})[42], and $LiNi_{0.5}Mn_{1.5}O_4$ (4.7 V, ca. 130 mAh g^{-1})[43].

Galvanostatic cycling at a rate of C/20 (Figure 4b) could deliver ca. 140 mAh g^{-1} reversibly without a noticeable change in the shape of the charge/discharge profile. At a faster rate of 1C, ca. 87% of the theoretical capacity of $Li_{1.1}Na_{0.4}VPO_{4.8}F_{0.7}$ could be retained after the first cycle. After 100 full charge–discharge cycles at 1C at room temperature, no significant capacity loss occurred (i.e., a capacity retention of 96%), as shown in the bottom panel of Figure 4c. Moreover, the cyclability at 60°C was even better: 98% of the initial capacity was sustained after 100 cycles (top panel of Figure 4c). The high cycle stability at elevated temperatures presents a clear advantage over its strongest competitor as a 4 V cathode material, the spinel $LiMn_2O_4$, which typically suffers from poor cycle performance at elevated temperatures due to severe manganese dissolution[44]. The outstanding cyclability of $Li_{1.1}Na_{0.4}VPO_{4.8}F_{0.7}$, irrespective of the operating temperature, implies high structural stability of the host framework.

Exceptionally high rate capability could be achieved for both charging and discharging of the $Li_{1.1}Na_{0.4}VPO_{4.8}F_{0.7}$ electrode (Figure 4d and 4e). At the 10C rate, more than 115 mAh g^{-1} could still be achieved. A capacity of ca. 100 mAh g^{-1} was obtained at the 25C rate. Moreover, similar capacities can be charged at the same current densities. This fast-charging capability is quite impressive given that the upper bound of the voltage window is 4.5 V, which is only ca. 0.5 V above the equilibrium voltage. Also, micron-sized particles (inset of Figure 3a) were able to provide very good power. Such a high rate capability had never been reported for any fluorophosphate-based electrodes to date, making $Li_{1.1}Na_{0.4}VPO_{4.8}F_{0.7}$ a promising candidate as a high-power cathode.

Discussion

We believe that the unexpected capacity retention (see Figure 4c) is due to the small difference in the cell volumes between lithiated and delithiated phases. The cell volumes of the pristine $Li_{1.1}Na_{0.4}VPO_{4.8}F_{0.7}$ and $Na_{0.4}VPO_{4.8}F_{0.7}$ (i.e., fully charged state) calculated from XRD experiments revealed that the change in volume between the two is ca. 0.7% (see Supplementary Figure S10 and Table S7). This unusually small volume change of $Li_{1.1}Na_{0.4}VPO_{4.8}F_{0.7}$ upon cycling is comparable to the lowest volume change reported for triplite $Li(Fe_{1-\delta}Mn_\delta)SO_4F$ (ca. 0.6%)[4]. First-principles structure calculations also confirmed the small volume difference between two simple models of $LiNa_{0.5}VPO_5F_{0.5}$ and $Na_{0.5}VPO_5F_{0.5}$ (see Chapter 9 in the Supplementary Information for calculation details). The structural investigation of $Li_{1.1}Na_{0.4}VPO_{4.8}F_{0.7}$ after 100 cycles at a rate of 1C rate showed no change in the XRD pattern (see Supplementary Figure S12).

The high rate capability of $Li_{1.1}Na_{0.4}VPO_{4.8}F_{0.7}$ (see Figure 4d and 4e) is attributable to fast Li^+ ion transport in the open crystal lattice

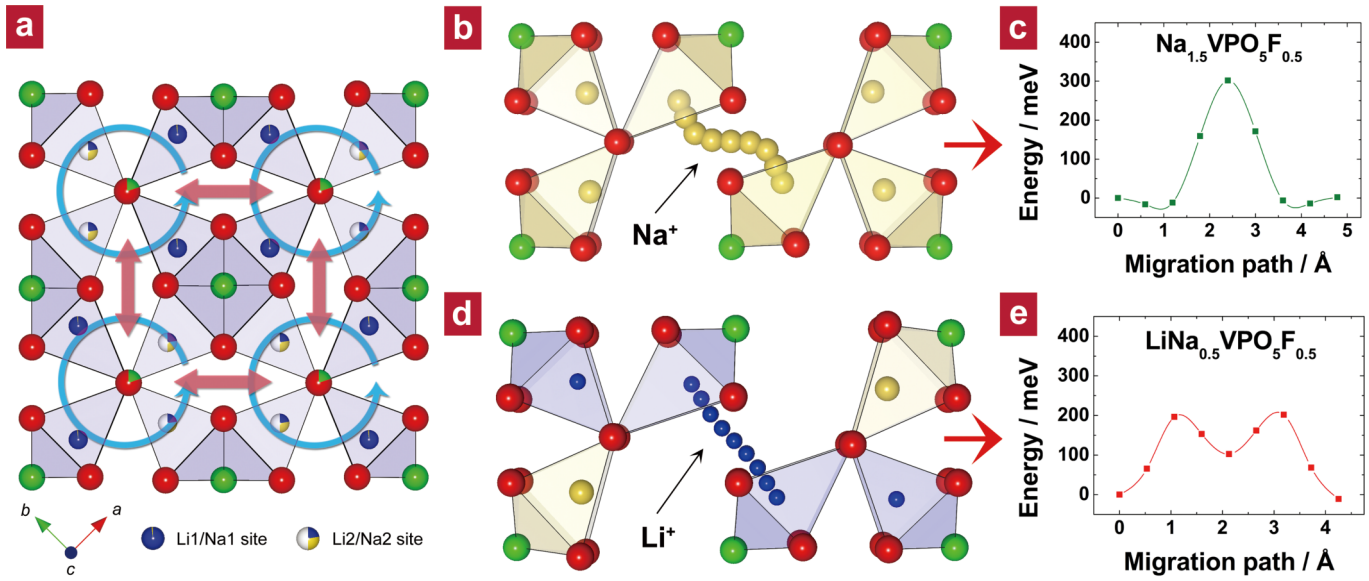

Figure 5 | NEB calculations for Na^+ and Li^+ diffusion in $Na_{1.5}VPO_5F_{0.5}$ and $LiNa_{0.5}VPO_5F_{0.5}$. (a) Top view (*ab* plane) of the alkali metal layer in $Li_{1.1}Na_{0.4}VPO_{4.8}F_{0.7}$, representing two types of diffusion paths for Li^+ ions (indicated by arrows). This illustration was based on the refinement results. Li, Na, O, and F atoms are represented in blue, yellow, red, and green, respectively. (b) Trajectories and (c) the corresponding activation barriers for Na hopping in diffusion path 2 in $Na_{1.5}VPO_5F_{0.5}$ as predicted by the NEB method. (d) Trajectories and (e) the corresponding activation barriers for Li hopping in diffusion path 2 in $LiNa_{0.5}VPO_5F_{0.5}$ as predicted by the NEB method. The Li^+ ion trajectory along path 2 is quite different from that of Na^+. While the Na^+ ions, whose site energy strongly affects the activation barrier, migrate with a sinusoidal motion (Figure 5b) along path 2 due to the small intermediate space in the middle of the path, the Li^+ ions travel in a nearly straight line (Figure 5d). The energy trajectory in Figure 5e indicates the metastability at the intermediate space. This is because the presence of Na^+ ions in the structure provides a larger empty space for Li^+ ions.

possessing two-dimensional diffusional pathways in the *ab* plane: Li^+ ions can hop along the ring-shaped route (path 1, circular cyan arrows in Figure 5a) or across the ring (path 2, straight red arrows in Figure 5a). Using the nudged-elastic-band (NEB) method[45,46], we estimated the diffusion kinetics of alkali ions for the two plausible diffusion paths (i.e., path 1 and path 2) with their activation energies (E_a). Two simplified models of $Na_{1.5}VPO_5F_{0.5}$ and $LiNa_{0.5}VPO_5F_{0.5}$ were introduced to examine the transport property of Na^+ ions and Li^+ ions in the isostructural $Na_{1.5}VPO_{4.8}F_{0.7}$ and $Li_{1.1}Na_{0.4}VPO_{4.8}F_{0.7}$, respectively (see Chapter 11 in the Supplementary Information for details on the NEB calculations). We found that a negligible E_a value at a similar scale of thermal energy at room temperature (ca. 25 meV) exists for both the Na^+ and Li^+ ions along path 1 (see Supplementary Figure S14). This implies unusually fast motion of these ions in the closed-loop ring pattern of the *ab* plane. Nevertheless, to escape or be reinserted into the material, the ions should be capable of crossing among ring patterns through path 2. The E_a values of diffusion path 2 for the Na^+ ions in $Na_{1.5}VPO_5F_{0.5}$ and Li^+ ions in $LiNa_{0.5}VPO_5F_{0.5}$ were estimated at 310 and 200 meV (Figure 5c and 5e), respectively (see Chapter 12 in the Supplementary Information for details on the corresponding diffusivity calculation). Since the extraction of Na^+ or Li^+ ions should involve both path 1 and path 2, the diffusion kinetics is rate-limited by the activation barrier for path 2. The activation barrier for Li hopping is significantly lower than that for Na hopping. This is probably because the residual Na^+ maintains a somewhat larger framework, which is beneficial for Li^+ ion diffusion in the lithium phase. The activation barrier for Li^+ ion hopping of $Li_{1.1}Na_{0.4}VPO_{4.8}F_{0.7}$ (200 meV) is even lower than that of $LiCoO_2$ (ca. 250 meV)[47,48], which gives an estimated diffusivity a few times greater than that for $LiCoO_2$. We believe that this is due to the smaller size of Li^+ ions compared to Na^+ ions, as well as the presence of partially-filled alkali-metal sites in the framework.

In this work, we have transformed a routine sodium compound into a promising fluorophosphate-based cathode material for lithium-ion batteries. We note that modifying polyanion groups to a significant extent while keeping the original structure intact is quite challenging, since the polyanion groups are often structural units of the crystal framework. Substantial substitution results in destruction of the original structure or the precipitation of a new phase. Here, tuning of the oxidation states of transition metals and their redox potentials was achieved by substantial ionic substitution in a polyanion group within a crystal structure. This tuning was crucial to enhancing its energy density as an electrode. The oxidation states of transition metals in the inorganic compounds may also be tuned by aliovalent cation doping[49]. However, in order to lower the initial oxidation state of V^{4+} in $Na_{1.5}VPO_5F_{0.5}$ via the aliovalent cation doping, elements having the valence of +5 or more need to be doped (or substituted) by substantial amounts. However, such cations are usually rare, unstable, or toxic (e.g. Cr^{6+}, Mn^{6+}, Nb^{5+}, Ta^{5+}, etc.). Also, those cations need to be strongly electronegative enough to reduce the valence of vanadium ion from +4 to +3 and electrochemically active at similar potential not to sacrifice the gravimetric capacity. Therefore, the fluorination replacing O^{2-} ions by F^- ions was a rational alternative. It is noteworthy that the modification of polyanion groups tailors not only the oxidation states of transition metals but also their redox potentials by affecting on the degree of the inductive effect.

In summary, a novel fluorophosphate-based electrode material having high energy and power capability with outstanding cycle stability was developed by tailoring a polyanion compound having an open framework. Once the synthesis of the electrode becomes optimized on the basis of cost, $Li_{1.1}Na_{0.4}VPO_{4.8}F_{0.7}$ will become a serious contender as a commercial electrode. The capacity of 156 mAh g^{-1} with a voltage of 4 V is comparable to other competitor cathode materials. The performance of our material even exceeds that of the recently discovered triplite $Li(Fe_{1-\delta}Mn_\delta)SO_4F$, which can deliver a theoretical capacity of 146 mAh g^{-1} with 3.90 V. Additionally, our material has excellent cycle stability and rate capability. The discovery of this new electrode material is particularly important because its energy density was tuned by tailoring the polyanion groups in the structure to widen the redox reaction range of the redox center. Such design flexibility broadens the scope for further

investigation of polyanion-based compounds as frameworks for new cathode materials and offers exciting opportunities for the development of new compounds.

Methods

Synthesis. A stoichiometric amount of V_2O_5 (Sigma-Aldrich, 99%) and $NH_4H_2PO_4$ (Sigma-Aldrich, 99%) was blended by high-energy ball-milling (HEBM) at 300 rpm over 24 hours. The mixture was then pelletized and heat-treated at 750°C for 4 hours in air to provide yellowish $VOPO_4$ (or $V^{5+}PO_5$) powder. A stoichiometric mixture of V_2O_5 and $NH_4H_2PO_4$, including 20 mol% Super P, was blended by HEBM at 300 rpm over 24 hours. Black VPO_4 powder was obtained by pelletizing and heat-treating the mixture at 850°C for 2 hours under an Ar atmosphere. The precursor combination used to synthesize $Na_{1.5}VPO_{5-\delta}F_{0.5+\delta}$ samples ($\delta = 0$, 0.2, and 1) was "$(1-\delta)V^{5+}PO_5 + \delta V^{3+}PO_4 + (0.5+\delta)$NaF (Sigma-Aldrich, 99%) + $[(1-\delta)/2]$ Na_2CO_3 (Sigma-Aldrich, 99%)". Blending was done by HEBM at 300 rpm for 24 hours; the resulting mixtures ($\delta = 0$, 0.2, and 1) were pelletized and sintered at 750°C for 1.5 hours under flowing argon to finally provide cyan-colored $Na_{1.5}VPO_5F_{0.5}$, greenish $Na_{1.5}VPO_{4.8}F_{0.7}$, and black $Na_{1.5}VPO_4F_{1.5}$ powders[50]. To prepare the isostructural lithium derivative of $Na_{1.5}VPO_{4.8}F_{0.7}$, we performed Na^+/Li^+ ion exchange in 1-hexanol (Sigma-Aldrich, 99%) at its boiling point (ca. 160°C) under reflux. LiBr (Sigma-Aldrich, 99%) was used as the lithium source. An excess amount (10 times) of LiBr was added prior to the reaction, and the volume of the solvent (i.e., 1-hexanol) was adjusted to make a 5 M LiBr solution. After reacting for 5–17 hours, the product was rinsed, centrifuged several times, and then thoroughly dried to provide green-colored $Li_{1.1}Na_{0.4}VPO_{4.8}F_{0.7}$ powder. To prepare the fully delithiated version of the $Li_{1.1}Na_{0.4}VPO_{4.8}F_{0.7}$ powder, it was oxidized with stoichiometric amounts of NO_2BF_4 in acetonitrile solvent at 60°C. After reaction for 10 hours, the product was washed, centrifuged several times with the same solvent, and then completely dried in a vacuum oven at 70°C overnight, resulting in a yellowish $Na_{0.4}VPO_{4.8}F_{0.7}$ powder.

Electron microscopy and elemental analysis. Transmission electron microscopy (TEM) images were acquired using a Tecnai F20 (FEI, USA) at an accelerating voltage of 200 kV. Scanning electron microscopy (SEM) images were obtained using a SUPRA 55VP FE-SEM (Carl Zeiss, Germany) at an operating voltage of 2 kV. Compositional analysis was carried out simultaneously with SEM examination by using energy-dispersive X-ray spectroscopy (EDS) (X-Flash spectrometer; Bruker, Germany) with a specified energy resolution of 127 eV at an operating voltage of 15 kV. For TEM observation, an EDAX/EDS system was used; all EDS measurements were repeated several times in different regions, and the observed values were averaged. The atomic ratios of lithium, sodium, vanadium, and phosphorus were more precisely determined by inductively coupled plasma (ICP) spectroscopy (Polyscan 60E; Thermo Jarrell Ash, USA). The carbon content of carbon-coated $Li_{1.1}Na_{0.4}VPO_{4.8}F_{0.7}$ was measured with a carbon–sulfur determinator (CS-800; ELTRA, Germany).

X-ray photoelectron spectroscopy. XPS spectra were obtained by electron spectroscopy for chemical analysis (ESCA) (Sigma Probe; Thermo VG Scientific, UK) with a pass energy of 30 eV and a step size of 0.1 eV. Binding energies were referenced to the C1*s* peak at 284.6 eV.

Diffraction. ND data were collected over a 2θ range of 0–180° with a step size of 0.05° and $\lambda = 1.83429$ Å supplied by a Ge(331) single-crystal monochromator on a high-resolution powder diffractometer (HRPD) at the Hanaro facility of the Korea Atomic Energy Research Institute. XRD was carried out using an X-ray diffractometer (D8 Advance; Bruker, Germany) using Ni-filtered Cu-Kα radiation ($\lambda = 1.5406$ Å) in the 2θ range of 10–80°. The room-temperature ND/XRD data were refined using the Rietveld method and Fullprof software[51]. Temperature-controlled XRD measurements were carried out under vacuum using an X-ray diffractometer (D/MAX-2500 diffractometer; Rigaku, Japan) with Cu-Kα radiation ($\lambda = 1.5406$ Å) and step scanning (0.01° s^{-1}) in the 2θ range of 10–60° with a scan speed of 2° min^{-1}. The heating rate was 5°C min^{-1}. Each measurement was taken after stabilizing at the desired temperature for ca. 3 min. Synchrotron powder XRD data were acquired at room temperature at the beam line of BL02B2 in SPring-8 (Japan) with an average wavelength of ca. 0.9988 Å calibrated using the NIST silicon fine powder (SRM640d).

NMR and EPR spectroscopy. Solid-state ^{6}Li and ^{23}Na MAS NMR spectroscopy experiments were performed using a Bruker Avance 400 MHz 9.4 T Wide Bore spectrometer at Larmor frequencies of 58.9 and 105.8 MHz, respectively; all experiments were performed with a Bruker 4-mm probe at a MAS frequency of 15 kHz at room temperature. For the ^{23}Na MAS NMR measurements, all spectra were obtained using a 90° pulse of 1 μs and a recycle delay of 0.5 s. The ^{6}Li MAS NMR spectra were collected using a 90° pulse of 2 μs and a recycle delay of 1 s. The ^{23}Na and ^{6}Li NMR shifts were referenced to 0.1 M NaCl (0 ppm) and 1 M LiCl (0 ppm), respectively. EPR spectra were recorded using a JES-TE200 electron spin resonance spectrometer (JEOL, Japan) at room temperature with 4-mm quartz tubes. The magnetic field was varied from 2000 to 5000 Gauss at a resonance frequency of 9.447 GHz.

Electrochemistry. For the electrochemical test, a slurry of 88 wt% carbon-coated $Li_{1.1}Na_{0.4}VPO_{4.8}F_{0.7}$ (70.4 wt% total active material), 2 wt% carbon black (19.6 wt% total carbon), and 10 wt% polyvinylidene fluoride (PVDF) dispersed in *N*-methyl-2-pyrrolidone (NMP) was prepared and cast on aluminum foil (see Chapter 13 in the Supplementary Information for details on the carbon-coating process). The electrode was dried overnight at 70°C under vacuum. The loading of the active material on the electrode was ca. 5–6 mg cm^{-2}. Electrochemical cells were assembled in an Ar-filled glove box into CR2016-type coin cells consisting of a counter electrode (lithium metal), separator (Celgard 2400; Celgard, USA), and electrolyte (1 M $LiPF_6$ solution) in a mixture of ethyl carbonate/dimethyl carbonate (EC/DMC, 1:1 v/v). All the electrochemical tests were carried out using a WBCS 3000 potentiostat (WonAtech, Korea). For the GITT measurement, the electrochemical cells were rested for 2 hours after each hour-long charging or discharging at the C/20 rate (voltage window: 2.2–4.5 V) at 60°C. 1C corresponds to 156 mA g^{-1}. To acquire the charge curves for various C rates, the cells were cycled once at the rate of C/20 and then charged to 4.5 V at different rates. To obtain the discharge curves for various C rates, the cells were charged at the same rate of C/20 to 4.5 V and then discharged to 2.5 V at different rates. Unless otherwise noted, all cells were cycled between 2.5 and 4.5 V at room temperature.

Computational details. First-principles calculations were made using the Perdew–Burke–Ernzerhof exchange-correlation parameterization to density functional theory (DFT) with the spin-polarized generalized gradient approximation (GGA)[52]. We used a plane-wave basis set and the projector-augmented wave (PAW) method as implemented in the Vienna *ab initio* simulation package (VASP)[53]. The Hubbard parameters (GGA+U)[54] were added to correct the incomplete cancellation of the self-interaction of GGA. A U value of 5.0 eV (the on-site coulomb term) and J value of 1.0 eV (the exchange term) were used for the vanadium ions[50,55] in $Na_{1.5}VPO_5F_{0.5}$, $LiNa_{0.5}VPO_5F_{0.5}$, and $Na_{0.5}VPO_5F_{0.5}$. Activation barriers for lithium and sodium diffusion in the two model systems of $Na_{1.5}VPO_5F_{0.5}$ and $LiNa_{0.5}VPO_5F_{0.5}$ were calculated using the nudged-elastic-band (NEB) method[56,57]. In those calculations, the Li^+ and Na^+ ions were allowed to move in $Na_{23/16}VPO_5F_{0.5}$ and $Li_{15/16}Na_{0.5}VPO_5F_{0.5}$. Seven replicas of the systems were used as the starting points for the NEB method with linear interpolation between the initial and final states of the path. All lattice parameters were fixed at the $Na_{1.5}VPO_5F_{0.5}$ and $LiNa_{0.5}VPO_5F_{0.5}$ states, but all the internal degrees of freedom were relaxed during the NEB calculations.

1. Tarascon, J. M. & Armand, M. Issues and challenges facing rechargeable lithium batteries. *Nature* **414**, 359–367 (2001).
2. Armand, M. & Tarascon, J. M. Building better batteries. *Nature* **451**, 652–657 (2008).
3. Recham, N. *et al.* A 3.6 V lithium-based fluorosulphate insertion positive electrode for lithium-ion batteries. *Nat. Mater.* **9**, 68–74 (2010).
4. Barpanda, P. *et al.* A 3.90 V iron-based fluorosulphate material for lithium-ion batteries crystallizing in the triplite structure. *Nat. Mater.* **10**, 772–779 (2011).
5. Tripathi, R., Popov, G., Ellis, B. L., Huq, A. & Nazar, L. F. Lithium metal fluorosulfate polymorphs as positive electrodes for Li-ion batteries: synthetic strategies and effect of cation ordering. *Energy Environ. Sci.* (2012).
6. Nishimura, S.-i., Nakamura, M., Natsui, R. & Yamada, A. New lithium iron pyrophosphate as 3.5 V class cathode material for lithium ion battery. *J. Am. Chem. Soc.* **132**, 13596–13597 (2010).
7. Nytén, A., Abouimrane, A., Armand, M., Gustafsson, T. & Thomas, J. O. Electrochemical performance of Li_2FeSiO_4 as a new Li-battery cathode material. *Electrochem. Commun.* **7**, 156–160 (2005).
8. Dominko, R. *et al.* Structure and electrochemical performance of Li_2MnSiO_4 and Li_2FeSiO_4 as potential Li-battery cathode materials. *Electrochem. Commun.* **8**, 217–222 (2006).
9. Kokalj, A. *et al.* Beyond one-electron reaction in Li cathode materials: Designing $Li_2Mn_xFe_{1-x}SiO_4$. *Chem. Mater.* **19**, 3633–3640 (2007).
10. Legagneur, V. *et al.* $LiMBO_3$ (M=Mn, Fe, Co): synthesis, crystal structure and lithium deinsertion/insertion properties. *Solid State Ionics* **139**, 37–46 (2001).
11. Abouimrane, A., Armand, M. & Ravet, N. in *203rd Meet. Electrochem. Soc. Ext. Abstr.* (2003).
12. Yamada, A. *et al.* Lithium iron borates as high-capacity battery electrodes. *Adv. Mater.* **22**, 3583–3587 (2010).
13. Barker, J., Saidi, M. Y. & Swoyer, J. Lithium metal fluorophosphate materials and preparation thereof. international patent WO01/084655 (2001).
14. Barker, J., Saidi, M. Y. & Swoyer, J. L. Electrochemical insertion properties of the novel lithium vanadium fluorophosphate, $LiVPO_4F$. *J. Electrochem. Soc.* **150**, A1394–A1398 (2003).
15. Ellis, B. L., Makahnouk, W. R. M., Makimura, Y., Toghill, K. & Nazar, L. F. A multifunctional 3.5 V iron-based phosphate cathode for rechargeable batteries. *Nat. Mater.* **6**, 749–753 (2007).
16. Makimura, Y., Cahill, L. S., Iriyama, Y., Goward, G. R. & Nazar, L. F. Layered lithium vanadium fluorophosphate, $Li_5V(PO_4)_2F_2$: A 4 V class positive electrode material for lithium-ion batteries. *Chem. Mater.* **20**, 4240–4248 (2008).
17. Recham, N. *et al.* Ionothermal synthesis of Li-based fluorophosphates electrodes. *Chem. Mater.* **22**, 1142–1148 (2009).
18. Nanjundaswamy, K. S. *et al.* Synthesis, redox potential evaluation and electrochemical characteristics of NASICON-related-3D framework compounds. *Solid State Ionics* **92**, 1–10 (1996).

19. Padhi, A. K., Nanjundaswamy, K. S. & Goodenough, J. B. Phospho-olivines as positive-electrode materials for rechargeable lithium batteries. *J. Electrochem. Soc.* **144**, 1188–1194 (1997).
20. Gaubicher, J., Wurm, C., Goward, G., Masquelier, C. & Nazar, L. Rhombohedral form of $Li_3V_2(PO_4)_3$ as a cathode in Li-ion batteries. *Chem. Mater.* **12**, 3240–3242 (2000).
21. Huang, H., Yin, S. C., Kerr, T., Taylor, N. & Nazar, L. F. Nanostructured composites: A high capacity, fast rate $Li_3V_2(PO_4)_3$/carbon cathode for rechargeable lithium batteries. *Adv. Mater.* **14**, 1525–1528 (2002).
22. Yin, S. C., Grondey, H., Strobel, P., Anne, M. & Nazar, L. F. Electrochemical property: Structure relationships in monoclinic $Li_{3-y}V_2(PO_4)_3$. *J. Am. Chem. Soc.* **125**, 10402–10411 (2003).
23. Chung, S.-Y., Bloking, J. T. & Chiang, Y.-M. Electronically conductive phospho-olivines as lithium storage electrodes. *Nat. Mater.* **1**, 123–128 (2002).
24. Ellis, B. L., Lee, K. T. & Nazar, L. F. Positive electrode materials for Li-ion and Li-batteries. *Chem. Mater.* **22**, 691–714 (2010).
25. Aono, H., Imanaka, N. & Adachi, G.-y. High Li^+ conducting ceramics. *Acc. Chem. Res.* **27**, 265–270 (1994).
26. Cushing, B. L. & Goodenough, J. B. $Li_2NaV_2(PO_4)_3$: A 3.7 V Lithium-insertion cathode with the rhombohedral NASICON structure. *J. Solid State Chem.* **162**, 176–181 (2001).
27. Goodenough, J. B., Hong, H. Y. P. & Kafalas, J. A. Fast Na^+-ion transport in skeleton structures. *Mater. Res. Bull.* **11**, 203–220 (1976).
28. Manthiram, A. & Goodenough, J. B. Lithium insertion into $Fe_2(SO_4)_3$ frameworks. *J. Power Sources* **26**, 403–408 (1989).
29. Sauvage, F., Quarez, E., Tarascon, J. M. & Baudrin, E. Crystal structure and electrochemical properties vs. Na^+ of the sodium fluorophosphate $Na_{1.5}VOPO_4F_{0.5}$. *Solid State Sci.* **8**, 1215–1221 (2006).
30. Huggins, R. A. *Advanced Batteries: Materials Science Aspects.* (Springer, 2008).
31. Ellis, B. L., Ramesh, T. N., Davis, L. J. M., Goward, G. R. & Nazar, L. F. Structure and electrochemistry of two-electron redox couples in lithium metal fluorophosphates based on the tavorite structure. *Chem. Mater.* **23**, 5138–5148 (2011).
32. Grey, C. P. & Dupre, N. NMR studies of cathode materials for lithium-ion rechargeable batteries. *Chem. Rev.* **104**, 4493–4512 (2004).
33. Tsirlin, A. A. *et al*. Phase separation and frustrated square lattice magnetism of $Na_{1.5}VOPO_4F_{0.5}$. *Phys. Rev. B* **84** (2011).
34. Poole, C. P. & Farach, H. A. *The Theory of Magnetic Resonance.* (Wiley-Interscience New York, 1972).
35. Slebodnick, C., Hamstra, B. & Pecoraro, V. in *Structure & Bonding* Vol. 89, *Modeling the Biological Chemistry of Vanadium: Structural and Reactivity Studies Elucidating Biological Function* (eds Hill, H., Sadler, P. & Thomson, A.) 51–108 (Springer Berlin/Heidelberg, 1997).
36. Yin, S. C., Strobel, P. S., Grondey, H. & Nazar, L. F. $Li_{2.5}V_2(PO_4)_3$: A room-temperature analogue to the fast-ion conducting high-temperature γ-phase of $Li_3V_2(PO_4)_3$. *Chem. Mater.* **16**, 1456–1465 (2004).
37. Clearfield, A. Role of ion-exchange in solid-state chemistry. *Chem. Rev.* **88**, 125–148 (1988).
38. England, W. A., Goodenough, J. B. & Wiseman, P. J. Ion-exchange reactions of mixed oxides. *J. Solid State Chem.* **49**, 289–299 (1983).
39. Tarascon, J.-M. *et al.* Hunting for better Li-based electrode materials via low temperature inorganic synthesis. *Chem. Mater.* **22**, 724–739 (2009).
40. Cho, J., Kim, Y. J., Kim, T.-J. & Park, B. Zero-strain intercalation cathode for rechargeable Li-ion cell. *Angew. Chem. Int. Ed.* **40**, 3367–3369 (2001).
41. Huang, H., Yin, S. C. & Nazar, L. F. Approaching theoretical capacity of $LiFePO_4$ at room temperature at high rates. *Electrochem. Solid-State Lett.* **4**, A170–A172 (2001).
42. Kim, D. K. *et al*. Spinel $LiMn_2O_4$ nanorods as lithium ion battery cathodes. *Nano Lett.* **8**, 3948–3952 (2008).
43. Lazarraga, M. G. *et al*. Nanosize $LiNi_yMn_{2-y}O_4$ ($0 < y < 0.5$) spinels synthesized by a sucrose-aided combustion method. Characterization and electrochemical performance. *J. Mater. Chem.* **14**, 1640–1647 (2004).
44. Xia, Y., Zhou, Y. & Yoshio, M. Capacity fading on cycling of 4 V $Li/LiMn_2O_4$ cells. *J. Electrochem. Soc.* **144**, 2593–2600 (1997).
45. Jonsson, H., Mills, G. & Jacobsen, K. W. in *Classical and Quantum Dynamics in Condensed Phase Simulations*. (eds Berne, B. J., Ciccotti, G. & Coker, D. F.) 385–404 (World Scientific Publishing Comany, 1998).
46. Meng, Y. S. & Arroyo-de Dompablo, M. E. First principles computational materials design for energy storage materials in lithium ion batteries. *Energy Environ. Sci.* **2**, 589–609 (2009).
47. Van der Ven, A., Ceder, G., Asta, M. & Tepesch, P. D. First-principles theory of ionic diffusion with nondilute carriers. *Phys. Rev. B* **64**, 184307 (2001).
48. Kang, K. & Ceder, G. Factors that affect Li mobility in layered lithium transition metal oxides. *Phys. Rev. B* **74**, 094105 (2006).
49. Chung, S.-Y., Bloking, J. T. & Chiang, Y.-M. Electronically conductive phospho-olivines as lithium storage electrodes. *Nat. Mater.* **1**, 123–128 (2002).
50. Shakoor, R. A., Seo, D.-H., Kim, H., Park, Y.-U., Kim, J., Kim, S.-W., Gwon, H., Lee, S. & Kang, K. A combined first principles and experimental study on $Na_3V_2(PO_4)_2F_3$ for rechargeable Na batteries. *J. Mater. Chem.* **22**, 20535–20541 (2012).
51. Roisnel, T. & Rodríguez-Carvajal, J. WinPLOTR: A windows tool for powder diffraction pattern analysis. *Mater. Sci. Forum* **378–381**, 118–123 (2001).
52. Perdew, J. P., Burke, K. & Ernzerhof, M. Generalized gradient approximation made simple. *Phys. Rev. Lett.* **77**, 3865–3868 (1996).
53. Kresse, G. & Furthmüller, J. Efficiency of ab-initio total energy calculations for metals and semiconductors using a plane-wave basis set. *Comput. Mater. Sci.* **6**, 15–50 (1996).
54. Anisimov, V. I., Zaanen, J. & Andersen, O. K. Band theory and Mott insulators: Hubbard U instead of Stoner I. *Phys. Rev. B* **44**, 943–954 (1991).
55. Tsirlin, A. A. *et al.* Phase separation and frustrated square lattice magnetism of $Na_{1.5}VOPO_4F_{0.5}$. *Phys. Rev. B* **84**, 014429 (2011).
56. Jonsson, H., Mills, G. & Jacobsen, K. W. in *Classical and Quantum Dynamics in Condensed Phase Simulations*. (eds Berne, B. J., Ciccotti, G. & Coker, D. F.) 385–404 (World Scientific Publishing Comany, 1998).
57. Meng, Y. S. & Arroyo-de Dompablo, M. E. First principles computational materials design for energy storage materials in lithium ion batteries. *Energy Environ. Sci.* **2**, 589–609 (2009).

Acknowledgements

This work was supported by the project of Global Ph.D. Fellowship which National Research Foundation of Korea had conducted since 2011. This work was also supported by the Fundamental R&D Program for Technology of World Premier Materials (WPM) and by Human Resources Development of the Korea Institute of Energy Technology Evaluation and Planning (KETEP) grant (20114010203120) funded by the Korea government Ministry of Knowledge Economy. This work was also supported by National Nuclear R&D Program through the National Research Foundation of Korea (NRF) funded by the Ministry of Education, Science and Technology (2012M2B2A4029335) and by the National Research Foundation of Korea Grant funded by the Korean Government (MEST) (NRF-2009-0094219). Support from Research Institute of Advanced Materials (RIAM) is also gratefully acknowledged. This work was also supported by the Supercomputing Center/Korea Institute of Science and Technology Information with supercomputing resources including technical support (KSC-2012-C2-45).

Author contributions

Y.-U. Park and R.A. Shakoor executed the synthesis with some advices from J.-M. Tarascon. The computational study was carried out by D.-H. Seo, and B.K. Kim carried out the NMR experiments. K.P. Hong, S. Lee, and H. Kim performed the ND analyses. Synchrotron XRD data were acquired by K. Miyasaka. K. Kang proposed the original idea and supervised the project. Y.-U. Park and K. Kang wrote the manuscript, and all authors participated in the discussion of the results and the structure of the final manuscript. Correspondence and requests for materials should be addressed to K. Kang.

Additional information

Supplementary information accompanies this paper at http://www.nature.com/scientificreports

Competing financial interests: The authors declare no competing financial interests.

How to cite this article: Park, Y.-U. *et al*. Tailoring a fluorophosphate as a novel 4 V cathode for lithium-ion batteries. *Sci. Rep.* **2**, 704; DOI:10.1038/srep00704 (2012).